Original Research

First-Principles Calculations of Structural, Lattice Dynamical, and Thermodynamic Properties of 4H-SiC

You Yu [1], Lijuan Tang [1], Caihong Liu [1], Shuhao Huang [1], Yanhong Shen [1], Yong Song [2], Zhiqiang Du [3], Ling Sun [1], Tixian Zeng [1,*]

[1] Information Materials and Device Applications Key Laboratory of Sichuan Provincial Universities, Chengdu University of Information Technology, Chengdu 610225, China;
[2] Institute of Applied Physics, Aba Teachers College, Aba 623002, China;
[3] Sichuan CSG Energy Saving Glass Co., Ltd., Chengdu 610299, China
* Correspondence: zengtx@cuit.edu.cn

Received: November 22, 2025; Accepted: January 27, 2026

Abstract: This study systematically investigates the structural, lattice dynamical, and thermodynamic properties of 4H-SiC using density functional theory (DFT), density functional perturbation theory (DFPT), and Boltzmann transport equation (BTE) frameworks. Using DFPT, we obtain the phonon frequencies and the phonon dispersion curves, as well as corresponding density of states. Quasi-harmonic approach was employed to analyze the thermodynamic parameters of 4H-SiC. The results reveal that the dynamically stable phonon spectrum provides a foundation for probing thermal transport mechanisms at high temperatures. BTE calculations demonstrate that the temperature-dependent lattice thermal conductivity originates from enhanced Umklapp scattering, with the nonlinear increase in the Grüneisen parameter quantitatively validated through relaxation-time approximations. The exceptional thermal stability is associated with its high thermal conductivity and the saturating behavior of the Grüneisen parameter at high temperatures, which suggests a suppression of strong anharmonic scattering. Correspondingly, the saturation of the thermal expansion coefficient at high temperatures is attributed to the weakened volume dependence of phonon frequencies. This work establishes an integrated first-principles workflow that provides a comprehensive self-consistent dataset across structural, lattice dynamical, and thermodynamic properties, offering theoretical guidance for optimizing 4H-SiC performance in extreme-environment applications.

Keywords: 4H-SiC; density functional theory; Boltzmann transport equation; lattice dynamical; thermodynamic

1. Introduction

As wide-bandgap indirect semiconductors, hexagonal silicon carbide polytypes display a band gap (~3.36 eV) that is approximately three times that of silicon (~1.12 eV) [1]. Among them, 4H-SiC exhibits a two-fold higher electron drift velocity and a three-fold higher thermal conductivity compared to Si [1–3]. 4H-SiC polytypes have demonstrated superior performance under harsh conditions, including high temperatures, elevated power, strong radiation, and high electric field strengths and frequencies [4–7]. Its exceptional thermal conductivity enables applications that require efficient heat dissipation, such as power electronics and high-power radio frequency devices. The effective thermal management capability enhances device performance and reliability [8], making 4H-SiC an ideal material for extreme-environment electronics. Owing to its hexagonal, layered structure, 4H-SiC exhibits unique lattice dynamics and thermodynamic properties. An in-depth investigation of the thermodynamic properties of 4H-SiC can deepen the fundamental understanding

of its material characteristics and provide a critical foundation for its advanced technological applications.

The thermal properties of materials are intrinsically governed by their atomic vibrational behavior. As quantized quasiparticles of lattice vibrations, phonons serve as the fundamental determinant of macroscopic thermomechanical characteristics in materials. Recent advancements in defect engineering have substantially enhanced charge carrier mobility [8], enabling high-performance power electronics. Concurrently, progress in phonon engineering [9,10] combined with machine learning-derived interatomic potential models [11] has facilitated precise prediction and optimization of thermal conductivity. Furthermore, 4H-SiC exhibits exceptional radiation resistance and high-temperature stability, positioning it as a promising material for nuclear fusion reactors [12].

Despite progress in the research on 4H-SiC, several challenges persist in accurately understanding its phonon spectrum, thermal conductivity k, free energy F, entropy S, heat capacity C, coefficient of thermal expansion (CTE) α, and the correlations among these characteristics. Notably, discrepancies emerge in 4H-SiC property calculations from different theoretical methods, highlighting the need for a unified and consistent dataset derived from a single computational framework. This study was motivated by the need for a consistent and comprehensive dataset to inform the design of 4H-SiC devices under extreme operating conditions, as required by our applied research projects. In this work, we develop a consistent computational workflow combining density functional theory (DFT), density functional perturbation theory (DFPT), and Boltzmann transport equation (BTE) for systematic analysis of 4H-SiC properties. Our results establish quantitative correlations between phonon transport and key macroscopic thermal properties, such as thermal conductivity, thermal expansion coefficient, and entropy, thereby providing theoretical foundations for optimizing 4H-SiC performance in extreme-environment applications.

2. Theory

In dielectric materials, thermal conductivity is predominantly governed by atomic vibrations. Using the BTE, Peierls established the foundational framework for describing thermal transport in dielectrics as the propagation and scattering of phonon gases [10]. This kinetic phonon gas model (PGM) has established the theoretical framework for understanding thermal conduction in crystalline solids. Phonon transport constitutes the primary heat conduction mechanism in semiconductors and insulators, which is especially true in 4H-SiC. The thermal conductivity k of crystalline materials is intrinsically limited by phonon scattering mechanisms arising from anharmonicity (phonon–phonon interactions), structural defects, isotopic disorder, and dopant impurities. A non equilibrium phonon distribution emerges under an applied temperature gradient, driving the diffusive propagation of phonons through the lattice [13].

As demonstrated by Peierls, heat transport in crystalline solids can be fundamentally understood as the propagation of phonons and their mutual scattering [10]. Among these processes, three-phonon interactions represent the lowest-order and typically dominant scattering mechanism. These interactions are classified into moment-conserving normal scattering and Umklapp scattering [14] that violates momentum conservation. Crucially, Umklapp scattering leads to intrinsic thermal resistance, imposing a fundamental limit on lattice thermal conductivity [14]. By identifying the characteristic timescale (known as the relaxation time or lifetime), τ, at which phonon-scattering events occur, we can generally formulate the thermal conductivity of a solid material as an integral on the phonon spectrum [9]:

$$k = \frac{1}{3}\int h\omega N(\omega)\frac{\partial f}{\partial T}v^2(\omega)\tau(\omega)d\omega = \frac{1}{3}\int C(\omega)v^2(\omega)\tau(\omega)d\omega \quad (1)$$

where $\int d\omega$ is integration over the entire phonon spectrum that sums over all polarizations, $\hbar$ represents the reduced Planck constant, ω signifies the lattice vibration frequency, $N(\omega)$ is the phonon density of states (DOS), f indicates the Bose-Einstein distribution, v represents the phonon group velocity, and $C(\omega) = h\omega N(\omega)\frac{\partial f}{\partial T}$ denotes the spectral volumetric specific heat.

The Grüneisen parameter (γ) quantifies how sensitive phonon frequencies are to unit cell volume changes, serving as a key link between lattice volume variations and phonon dynamics. A positive γ means phonon frequencies decrease as volume increases, with its magnitude reflecting the strength of this response. This parameter directly governs the coupling between thermal expansion and anharmonic scattering, underpinning the analysis of temperature-dependent properties like lattice thermal conductivity and CTE [14]. It is defined as:

$$\gamma = -\frac{\partial \ln \omega}{\partial \ln V} \tag{2}$$

where V represents the volume.

The knowledge of the entire phonon spectrum granted by DFPT makes possible the calculation of several important thermodynamic properties as functions of temperature T. In a quasi-harmonic approach, the free energy F of a system at temperature T and volume V is given by [15]:

$$F = E_0(V) + F_{vib}(V,T) \tag{3}$$

where $E_0(V)$ is the static energy at 0 K and a certain volume V, and $F_{vib}(V, T)$ represents the vibrational contribution to free energy. After calculating the free energy F, the heat capacity at constant volume (C_V) and the heat capacity at constant pressure (C_P) can be determined through [15]:

$$C_V = 3nNk_B\int_0^\infty \ln\left\{\left(\frac{h\omega}{2k_BT}\right)^2 \operatorname{csch}^2\left(\frac{h\omega}{2k_BT}\right)\right\} g(\omega)d\omega \tag{4}$$

$$C_P = C_V + \alpha^2 BTV \tag{5}$$

where k_B indicates the Boltzmann constant, $g(\omega)$ indicates the normalized phonon density of states with $\int_0^\infty g_{(\omega)}d\omega = 1$. α represents the volumetric CTE, and B denotes the bulk modulus.

Entropy (S) serves as an important quantity in thermodynamic modeling that can be used to develop multi-component phase diagrams and understand the thermal vibration response of materials at high temperatures, which is typically estimated by [15]:

$$S = 3k_B\int_0^\infty \left[\frac{h\omega}{2k_BT}\coth\frac{h\omega}{2k_BT} - \ln\left(2\sinh\frac{h\omega}{2k_BT}\right)\right] g(\omega)d\omega \tag{6}$$

3. Computational method

This study performed DFT and DFPT calculations using the Vienna *Ab initio* Simulation Package (VASP) [16–18]. DFT was employed to compute the reference dataset energies, while DFPT computations were leveraged to obtain the harmonic force constants and phonon dispersions. The exchange-correlation functional was processed using the Perdew-Burke-Ernzerhof (PBE) variant of the generalized gradient approximation (GGA) [19], while Brillouin zone integration was conducted on a Monkhorst-Pack grid [20]. For structural optimization of 4H-SiC, an 8 × 8 × 4 k-mesh was employed to relax the lattice constants and atomic positions. The valence electron configurations of carbon ($2s^22p^2$) and silicon ($3s^23p^2$) were explicitly treated using the projector-augmented wave (PAW) [21] method. For higher calculation accuracy, we set the plane wave cutoff energy to 400 eV [16] and adopted energy and force convergence criteria of 1.0 × 10^{-8} eV/atom and 0.01 eV/A, respectively.

The DFPT method was adopted for phonon calculations. We employed Phonopy [22] to compute the second-order force constants, using a 3 × 3 × 1 supercell expansion to ensure comparable lattice parameters (a and c) of 4H-SiC, forming a near-regular hexagonal unit cell that reduces anisotropy and approximates a cubic shape for more balanced treatment of directions. the third-order force

constants were also calculated using DFPT within the same 3 × 3 × 1 supercell to maintain consistency. These calculations were performed within the DFPT framework as implemented in VASP. The third-order force constants tensor was symmetrized using the thirdorder.py code [23,24], and the phonon BTE was solved using ShengBTE software [23], which obtained the lattice thermal conductivity. A uniform *q*-grid spacing was maintained for computation accuracy. After the convergence test, the grid size for 4H-SiC was set to 23 × 23 × 7, ensuring fine sampling of the Brillouin zone and improved numerical precision.

4. Results and discussion

4.1. Structural optimization

The 4H-SiC unit cell has a hexagonal structure composed of alternating layers with 4 silicon and 4 carbon atoms, which form a three-dimensional covalent lattice [4], and its space group is classified as P63mc. Constructing an accurate 4H-SiC cell model is critical for elucidating its physical properties and intrinsic mechanisms. As illustrated in Figure 1, the structural model serves as the fundamental building block of the 4H-SiC crystal. Within each Si-C bilayer, tetrahedral coordination is observed. In other words, each silicon atom is covalently bonded to 4 carbon atoms, and vice versa. This rigid tetrahedral coordination framework imparts exceptional stability and mechanical strength to 4H-SiC.

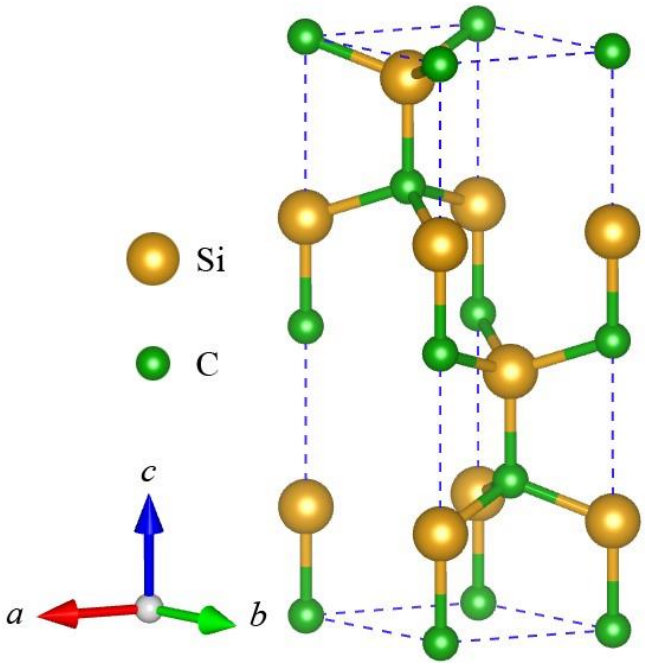

Figure 1. Structural model of 4H-SiC.

The lattice parameters of 4H-SiC are listed in Table 1 (Ref. [4,11,25–29]), which compiles calculated values from various theoretical methods [4,11,25,26] and experimental measurements [27–29]. Geometric optimization within the GGA framework yields lattice constants of a = 3.093 Å and c = 10.133 Å, which show maximum deviations of 0.8% from theoretical values and 0.6% from experimental results. These minor discrepancies arise from the GGA-PBE functional effects, which induce a systematic overestimation of lattice constants [30]. Nevertheless, the consistency across methods validates the reliability of GGA for structural predictions. Consequently, the optimized parameters are adopted for subsequent property calculations.

Table 1. Lattice parameters of 4H-SiC.

Method	*a* (Å)	*c* (Å)	*c*/*a*
DFT-PBE (Present work)	3.093	10.133	3.276
DFT-PBE (Ref. [11])	3.093	10.127	3.274
DFT-LDA (Ref. [4])	3.075	10.054	3.270
DFT-HSE06 (Ref. [25])	3.057	10.014	3.275
VFFM (Ref. [26])	3.073	10.053	3.271
Exp. (Ref. [27])	3.079	10.081	3.274
Exp. (Ref. [28])	3.081	10.061	3.265
Exp. (Ref. [29])	3.076	—	—

4.2. Lattice dynamics

The calculated phonon dispersion curves along high-symmetry paths in the Brillouin zone and the corresponding phonon DOS of 4H-SiC are shown in Figure 2. The abscissa of the dispersion curves represents the reduced wave vector, covering partial high-symmetry points, which characterize phonon behavior at distinct wave vector positions. The ordinate of the dispersion curves denotes the phonon frequency in terahertz (THz), spanning the full frequency range of vibrational modes in 4H-SiC. A crystal lattice with n atoms per unit cell has $3n$ branches, three of which are acoustic (LA+2TA) and the remainder are optical. With eight atoms in the primitive unit cell of 4H-SiC one expects twenty-four branches at Γ point. As the wave vector of the mode approaches zero, the acoustic sum rule (ASR) ensures that all acoustic mode frequencies approach zero. Inclusion of the long range polarization interaction results in splitting of the modes into LO and TO components. An interesting acoustic branching feature is found near Γ point, where low frequency optical modes are slightly entangled with acoustic modes, especially in the Γ-A and Γ-M directions. You can see that there is a significant gap between the twelve upper energy branches and the remaining twelve dispersion branches. The calculated phonon spectrum aligns with previous studies, particularly in the Γ-point frequency values [13,25]. This consistency validates the adopted computation model and parameters.

The steep slopes of the low-wavevector acoustic branches and low-frequency optical branches in the phonon dispersion curves indicate high group velocities. The low-frequency acoustic phonons, acting as the dominant carriers of lattice thermal energy, underpin the exceptional thermal conductivity of 4H-SiC. Notably, the restricted phase space for Umklapp scattering in 4H-SiC is a consequence of its high lattice symmetry and weak anharmonicity. This effect, however, is confined to low-wavevector, high-frequency acoustic phonons rather than applying to all high-frequency modes. By contrast, high-frequency optical phonons have low group velocities and strong intrinsic scattering, contributing negligibly to thermal transport. This targeted scattering suppression in low-wavevector high-frequency acoustic phonons further supplements thermal transport enhancement [31].

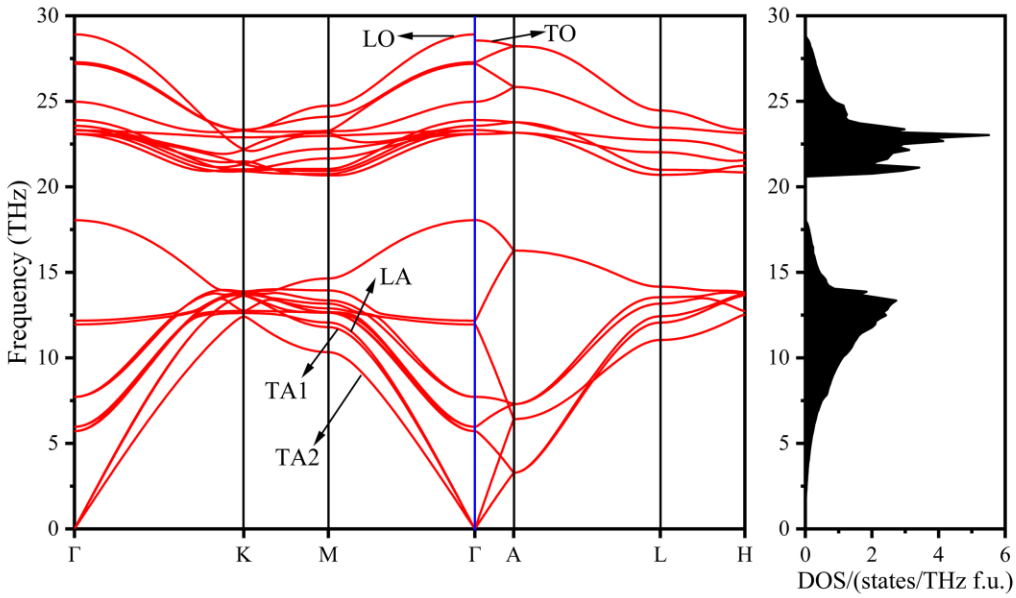

Figure 2. Calculated phonon dispersion curves along high-symmetry lines in the Brillouin zone and corresponding phonon DOS for 4H-SiC.

In the phonon spectrum of 4H-SiC, the phonon frequency ω is fundamentally related to the vibrational energy and the restoring forces between atoms. Within the harmonic approximation, the square of this frequency, ω^2, serves as a direct measure of the force constants, thereby quantifying the stiffness of the atomic bonds. The dynamical stability of the crystal is confirmed by the fact that all values of ω^2 are positive across the entire Brillouin zone, which results in exclusively real vibrational frequencies and indicates that all vibrational modes are stable. Conversely, the emergence of imaginary frequencies, which arise from negative ω^2 values, would signal a dynamical instability and correspond to vibrational modes that drive the structure towards distortion [32]. As shown in Figure 2, the absence of imaginary frequencies in the phonon spectrum of 4H-SiC indicates that the current crystal structure is dynamically stable. This observation confirms that atomic displacements from equilibrium positions are negligible, and no structural distortions occur under the studied conditions.

The phonon DOS is plotted with its magnitude on the abscissa and frequency on the ordinate, representing the population of phonon modes per unit frequency. A direct correspondence exists between phonon dispersion and DOS. Specifically, regions with densely packed frequency branches in the dispersion spectrum exhibit a higher DOS, signifying a greater density of vibrational states. This consistency between the dispersion and DOS demonstrates the structural regularity of 4H-SiC, where atomic arrangements follow a well-defined hexagonal symmetry. The absence of localized anomalous modes in the DOS spectrum further confirms that atomic vibrations adhere to the crystal lattice periodicity within the harmonic approximation [33].

4.3. Lattice thermal conductivity

The mode-dependent Grüneisen parameter were averaged over the entire phonon spectrum using the heat capacity weighting method to obtain the macroscopic Grüneisen parameter presented in Figure 3. At low temperatures, this averaged parameter is primarily governed by acoustic and low-frequency optical phonon branches, whereas high-temperature behavior is dominated by optical phonons [34]. The averaged parameter exhibits a week temperature dependence (changing from 1.051 at 100 K to 1.061 at 1200 K), which is consistent with the saturating behavior of anharmonicity at high temperatures.

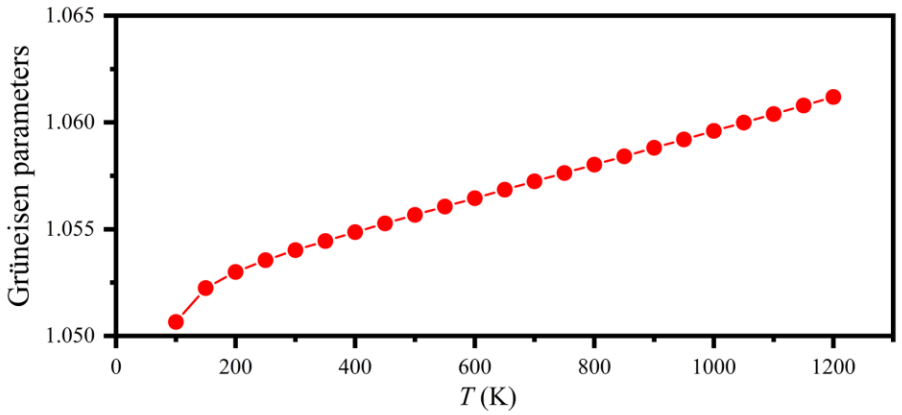

Figure 3. Grüneisen parameter variations with temperature for 4H-SiC.

The slightly increasing Grüneisen parameter amplifies the sensitivity of phonon frequencies to volumetric variations, thereby intensifying Umklapp scattering [35]. This anharmonic mechanism shortens phonon lifetimes and reduces lattice thermal conductivity. Within the medium-to-high temperature range (300–800 K), the phonon-phonon scattering regulated by the Bose-Einstein distribution intensifies, which significantly shortens the average phonon free path and further leads to a rapid decline in thermal conductivity. This trend is consistent with the temperature-dependent thermal conductivity of 4H-SiC shown in Figure 4 and has been verified by both experimental and computational methods [35]. The compiled dataset reveals a consistent thermal conductivity reduction with rising temperature across all methods. Notably, above 500 K, the lattice thermal conductivity maintains a monotonic decrease, consistent with the dominance of intrinsic Umklapp scattering. The apparent flattening of the curve corresponds to a reduction in the rate at which the thermal conductivity decreases. This trend is consistent with the saturating trend of the Grüneisen parameter at high temperatures. The saturation of the Grüneisen parameter suggests a moderation in the increase of anharmonicity, which aligns with the observed moderation in the enhancement of phonon scattering rates governing the thermal conductivity decay [14].

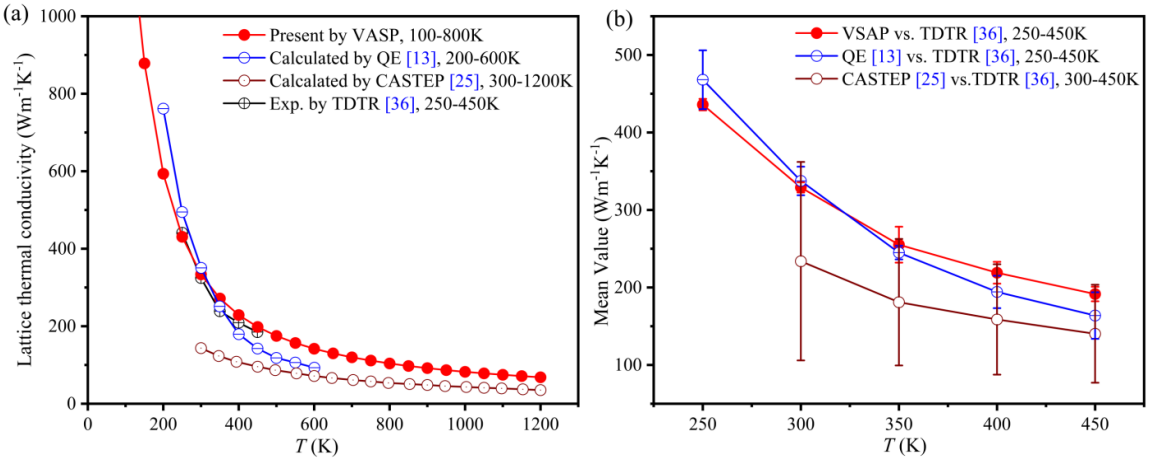

Figure 4. (a) Lattice thermal conductivity of 4H-SiC versus temperature, compared with calculated and experimental values; (b) mean error of computed values from different methods relative to experimental reference.

The overall trend and magnitude of the calculated thermal conductivity exhibit excellent agreement with established first-principles benchmarks reported in the literature. This consistency validates the present computational protocol for capturing the intrinsic phonon scattering physics. The distinctive contribution of this work, however, lies in the establishment of a unified first-

principles framework that delivers a fully consistent dataset across multiple properties—spanning structural, lattice dynamical, and thermodynamic domains—rather than in the recomputation of any single property. The accurate prediction of thermal conductivity within this integrated approach underscores its robustness for comprehensive material characterization.

We compared our computational results with thermal conductivity data derived from Quantum ESPRESSO (QE) [13] and CASTEP [25] simulations, alongside experimental measurements acquired via the time-domain thermoreflectance (TDTR) method [36]. Our calculated values also show good agreement with the experimental data from TDTR [36]. Notably, systematic discrepancies emerge among these results. Although VASP, QE, and CASTEP are all rooted in first-principles DFT, their divergent approaches to electronic structure approximations-including exchange-correlation functionals and basis set formulations-result in systematic variations in thermal conductivity predictions. These discrepancies stem from differences in the treatment of electron-phonon coupling strengths and phonon dispersion relations, which critically govern lattice thermal transport. Furthermore, deviations between the experimental TDTR data and theoretical predictions arise from oversimplified computational models that omit intrinsic material heterogeneities.

To quantify these systematic discrepancies, panel (b) of Figure 4 presents the mean error of each computational method relative to the TDTR experimental data over their comparable temperature intervals. The positive mean errors indicate a general overestimation of thermal conductivity by the DFT-based methods. This overestimation can be attributed to the inherent approximations in the exchange-correlation functionalsand the basis sets used across different codes, which collectively influence the calculated phonon dispersion relations and scattering rates. Additionally, the idealized defect-free crystal models in simulations neglect the phonon scattering from point defects, dislocations, and isotopic disorders present in real samples, further contributing to the discrepancy with experiments.

Throughout the investigated temperature range, 4H-SiC exhibits remarkably high thermal conductivity, demonstrating exceptional heat transfer capabilities. The thermal stability under elevated temperatures further highlights its robust performance retention. These properties position 4H-SiC as a promising candidate for high-power-density applications, including power electronics and thermal management systems requiring reliable operation in extreme thermal environments.

The high thermal conductivity of 4H-SiC and its retention at elevated temperatures (Figure 4) indicate efficient phonon transport. The saturating trend of the macroscopic Grüneisen parameter (Figure 3) further suggests that anharmonic scattering does not intensify drastically, a behavior often linked to the contribution of optical phonons with weaker anharmonicity. This interpretation is supported by prior studies on SiC polytypes [13,31], which attribute significant thermal conductivity to high-frequency optical modes.

4.4. Free energy, entropy, and heat capacity

The thermodynamic properties of 4H-SiC calculated within DFPT are determined by phonon calculations based on the quasi-harmonic approximation. Figure 5 illustrates the temperature-dependent free energy profile of 4H-SiC across a broad thermal range (100–1800K). The data for the red curve are obtained from first-principles calculations carried out in this study using the VASP code with the Perdew-Burke-Ernzerhof (PBE) functional. For comparative analysis, the data from three different computational methods reported in other literatures are also presented [11,37,38]. All calculated free energy curves exhibit a monotonic decrease with rising temperature, consistent with the fundamental thermodynamic relation.

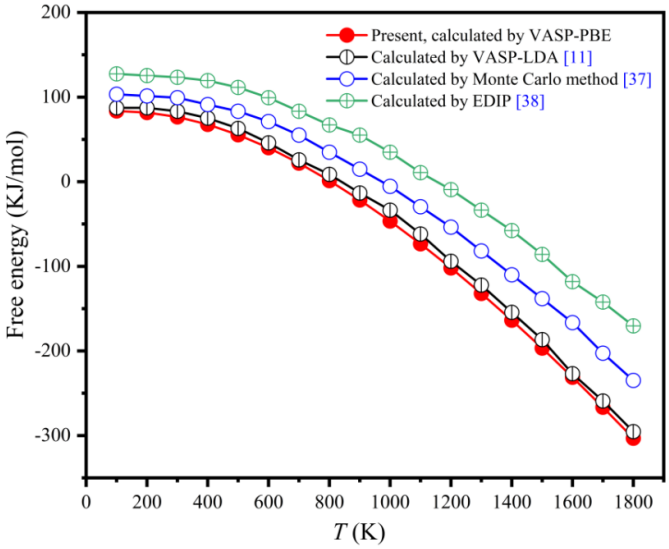

Figure 5. Free energy of 4H-SiC as a function of temperature, compared with other calculated values.

The entropy (S) discussed here primarily originates from atomic vibrations, a thermodynamic quantity characterizing the disorder of a system, is intrinsically linked to the number of accessible microscopic configurations. As shown in Figure 6, the entropy of 4H-SiC exhibits a monotonic increase across the studied temperature range (100–1800 K), consistent with those characterized in the other three approaches. This agreement underscores the universal trend of entropy growth driven by enhanced atomic vibrational freedom and configurational disorder at elevated temperatures.

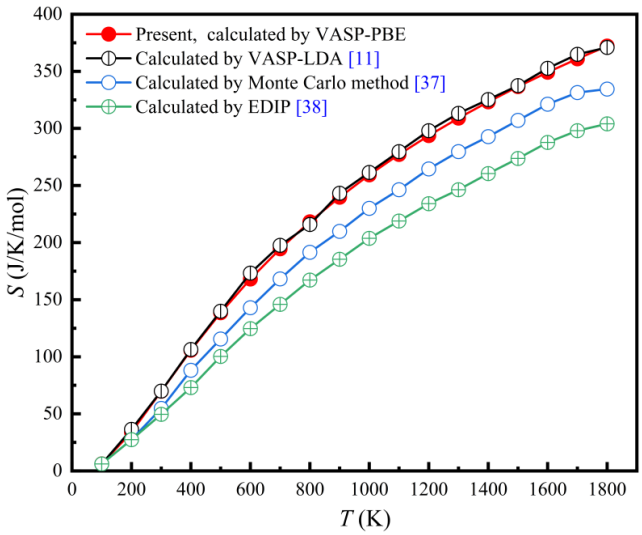

Figure 6. Entropy of 4H-SiC as a function of temperature, compared with other calculated values.

Heat capacity is a measure of how easily a substance absorbs or releases heat as the temperature varies, reflecting its ability to store heat. Figure 7 illustrates the C_V and C_p values of 4H-SiC as functions of temperature. We compared the C_p values calculated from the same VASP simulation approach and the experimental method of differential scanning calorimetry (DSC) [39], which exhibit consistent trends and small errors. C_V and C_p display similar temperature-dependent trends, showing monotonic increases with gradually diminishing rates at higher temperatures. C_V increases rapidly when the temperature is below 600 K, which is in line with the famous Debye model. Over 600 K, the isochoric heat capacity increases slowly with temperature and approaches a stable value (Dulong-Petit limit). In this case, $C_V = 3nR$, where n is the amount of substance, and R represents the gas

constant (8.314 J·mol^{-1}·K^{-1}). In solids, the difference between C_P and C_V originates from thermal expansion and elastic work contributions, as described by the thermodynamic framework for condensed phases [15]. While C_V reaches a plateau at elevated temperatures, C_P converges toward this stabilized value yet remains consistently higher. This fundamental relationship dictates that 4H-SiC absorbs greater heat under constant-pressure conditions compared to constant-volume conditions for an equivalent temperature increase.

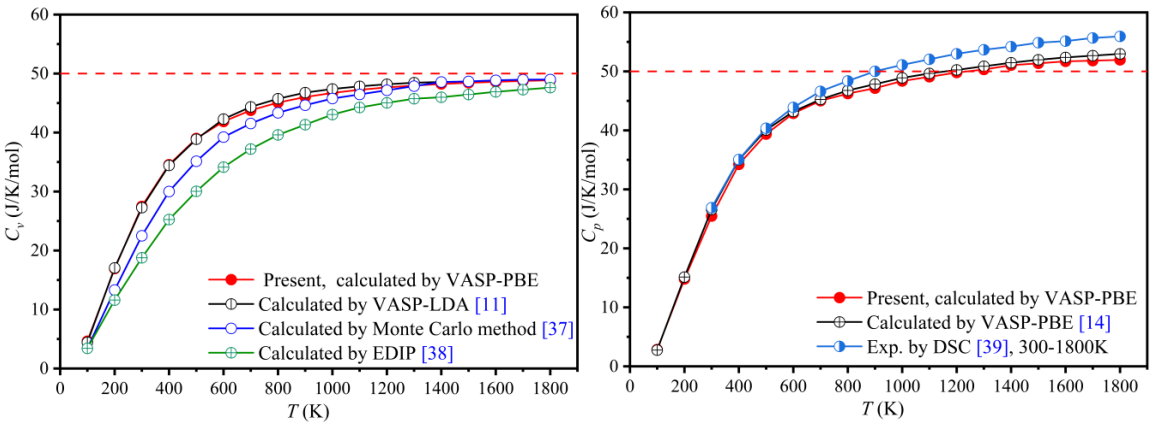

Figure 7. C_V and C_P values of 4H-SiC as functions of temperature.

In the graphs showing the temperature dependence of entropy, free energy, and constant-volume heat capacity, a slight difference exists between the calculated results of PBE and LDA [11]. This is because their different processing strategies of exchange-related functionals directly affect the electronic structure and phonon spectrum, thereby altering the temperature dependence of free energy. In VASP calculations, perfect crystal structures are typically assumed, ignoring microstructural changes (e.g., defects and dislocations) that may occur at high temperatures. The Metropolis Monte Carlo method directly simulates the configuration space of the system through statistical sampling. In contrast, the EDIP approach relies on parameterized potential functions to describe interatomic interactions, enabling the simulation of larger systems. Although minor discrepancies exist among the results derived from different computational methodologies, all datasets consistently exhibit identical trends across the investigated temperature range.

4.5. Coefficient of thermal expansion

For hexagonal structures, the CTE coefficient can be calculated by $\alpha=V^{-1}(\partial V/\partial T)_P$ [15]. The CTE variations of 4H-SiC with temperature are shown in Figure 8. Both VASP and CASTEP calculations demonstrate that the CTE of 4H-SiC exhibits an initial linear increase with temperature, followed by a progressive reduction in growth rate at elevated temperatures [14,40]. The rising temperature amplifies atomic vibrations, and the nonharmonic effect causes increased equilibrium atom spacings and expanded crystal lattices. When the atoms vibrate away from the equilibrium position beyond a certain temperature, the asymmetry between the repulsive and attractive forces strengthens, resulting in a deceleration in the growth rate of the average atom spacing. Under the quasi-harmonic approximation, the flattening of CTE growth is dominantly driven by the saturation of the Grüneisen parameter—a key quantity that describes the sensitivity of phonon frequencies to volume changes and thus governs the coupling between atomic vibrations and lattice expansion. According to the quasi-harmonic approximation, the CTE is directly proportional to the Grüneisen parameter. At high temperatures, however, the Grüneisen parameter tends to saturate, diminishing the temperature-dependent shift in phonon frequencies that drives thermal expansion. Consequently, the rate of CTE increase slows down. While the stabilization of heat capacity at high temperatures (as shown in Figure 7) eliminates the possibility of CTE enhancement from increased vibrational energy input, it

only plays a secondary role in CTE flattening—without the saturation of the Grüneisen parameter, CTE would still tend to rise even if heat capacity stabilizes.

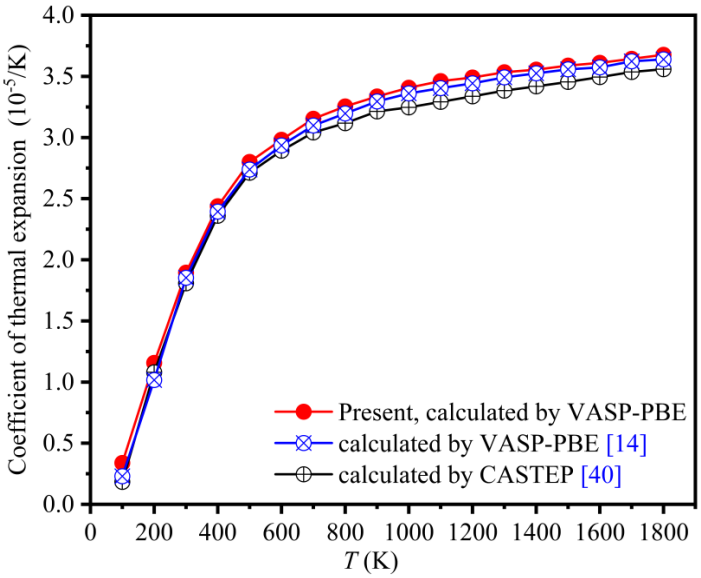

Figure 8. CTE of 4H-SiC versus temperature.

5. Conclusions

In this study, we employed first-principles calculations using VASP combined with Phonopy and ShengBTE to provide a systematic and consistent investigation of the phonon spectrum, thermal conductivity, and thermodynamic properties of hexagonal 4H-SiC polytypes. By integrating these calculations, we establish quantitative correlations between the microscopic lattice dynamics and key macroscopic thermal properties, thereby addressing inconsistencies found in the literature and providing a reliable, unified dataset for device design. Despite decreasing with temperature, the thermal conductivity of 4H-SiC starts from a large initial value and remains high over a broad temperature range, enabling effective heat dissipation. The variations of temperature-dependent entropy and free energy also endow 4H-SiC with good stability at high temperatures. Moreover, the increasing heat capacity of 4H-SiC with temperature demonstrates its promise for efficient energy storage in thermal management systems. Since the CTE increases with temperature, when designing 4H-SiC-based precision devices, we must consider dimensional variations due to temperature changes and compensate or control the thermal expansion to ensure accuracy. Beyond these general considerations, the consistent thermodynamic dataset provided in this work offers critical inputs for applied design and process optimization. This consistent dataset provides critical inputs for applied design. The CTE data enables thermal stress analysis in hetero-integrated systems to prevent CTE-mismatch-induced delamination. The heat capacity is vital for predicting transient thermal behavior in high-power devices. Furthermore, these properties are essential for thermo-mechanical models that optimize crystal growth processes like PVT to reduce defects. In summary, the unique structural, lattice dynamical, and thermodynamic properties of 4H-SiC enable its widespread application in modern semiconductor technology, holding both fundamental scientific insights and practical value.

This study establishes a comprehensive multiscale computational approach that DFT, DFPT, and the BTE to elucidate the structural, lattice dynamical, and thermodynamic properties of 4H-SiC. In contrast to prior works that often report on isolated properties, our approach provides a coherent dataset derived from a single computational chain that quantitatively links the microscopic phonon transport mechanisms to key macroscopic thermal behaviors, including thermal conductivity, heat capacity, entropy, free energy, and thermal expansion coefficient. This systematic integration allows us to resolve inconsistencies found in the literature and offers a reliable benchmark for the design and simulation of 4H-SiC-based devices operating under extreme thermal conditions.

Acknowledgments: The authors thank TopEdit for professional English language editing.

Availability of Data and Materials: The authors confirm the data supporting the findings of this study are available within the article.

Funding: This work was supported by Sichuan Province Science and Technology Program (Grant nos. 2023ZYD0175, 2023YFG0074) and Aba Prefecture Science and Technology Program (No. R24YYJSYJ0002).

Author Contributions: LT and CL conceived and designed the calculation. SH and YHS performed the calculation. YS and ZD analyzed the data. LS and TZ contributed analysis tools. YY wrote the paper. All authors read and approved the final manuscript. All authors have participated sufficiently in the work and agreed to be accountable for all aspects of the work. All authors contributed to editorial changes in the manuscript.

Conflicts of Interest: Zhiqiang Du analyzed the data. Any work related to his affiliation has not been included in this article in any form. Zhiqiang Du is a member of Sichuan CSG Energy Saving Glass Co., Ltd.; he declares that there are no conflicts of interest. All other authors also declare that they have no conflicts of interest.

References

1. Eddy Jr, C.R.; Gaskill, D.K. Silicon carbide as a platform for power electronics. *Science* 2009, 324, 1398–1400. https://doi.org/10.1126/science.1168704
2. Ryu, S.H.; Krishnaswami, S.; Das, M.; et al. 2 KV 4H-SiC DMOSFETs for low loss, high frequency switching applications. *International Journal of High Speed Electronics and Systems* 2004, 14, 879–883. https://doi.org/10.1142/S0129156404002983
3. Schwierz, F.; Roschke, M.; Liou, J.J.; et al. Theoretical investigation of the electrical behavior of SiC MESFETs for microwave power amplification. *Materials Science Forum* 1998, 264–268, 973–976. https://doi.org/10.4028/www.scientific.net/MSF.264-268.973
4. Karch, K.; Pavone, P.; Windl, W.; et al. Ab initio calculation of structural, lattice dynamical, and thermal properties of cubic silicon carbide. *International Journal of Quantum Chemistry* 1995, 56, 801–817. https://doi.org/10.1002/qua.560560617
5. Park, C.H.; Cheong, B.H.; Lee, K.H.; et al. Structural and electronic properties of cubic, 2H, 4H, and 6H SiC. *Physical Review B* 1994, 49, 4485–4493. https://doi.org/10.1103/PhysRevB.49.4485
6. Käckell, P.; Wenzien, B.; Bechstedt, F. Influence of atomic relaxations on the structural properties of SiC polytypes from ab initio calculations. *Physical Review B* 1994, 50, 17037–17045. https://doi.org/10.1103/PhysRevB.50.17037
7. Konstantinova, E.; Bell, M.J.V.; Anjos, V. Ab initio calculations of some electronic and elastic properties for SiC polytypes. *Intermetallics* 2008, 16, 1040–1042. https://doi.org/10.1016/j.intermet.2008.06.003
8. Tan, C.S.; Des, C.G. Electrical conductivity improvement of point defects in 4H-SiC. *Crystal Growth & Design* 2023, 23, 6250–6257. https://doi.org/10.1021/acs.cgd.3c00611
9. Qian, X.; Zhou, J.W.; Chen, G. Phonon-engineered extreme thermal conductivity materials. *Nature Materials* 2021, 20, 1188–1202. https://doi.org/10.1038/s41563-021-00918-3
10. Peierls, R. Zur kinetischen Theorie der Wärmeleitung in Kristallen [On the kinetic theory of heat conduction in crystals]. *Annalen der Physik* 1929, 395, 1055–1101. https://doi.org/10.1002/andp.19293950803
11. Fu, B.Q.; Sun, Y.D.; Jiang, W.R.; et al. Determining the thermal conductivity and phonon behavior of SiC materials with quantum accuracy via deep learning interatomic potential model. *Journal of Nuclear Materials* 2024, 591, 154897. https://doi.org/10.1016/j.jnucmat.2024.154897
12. Koyanagi, T.; Katoh, Y.; Nozawa, T.; et al. Recent progress in the development of SiC composites for nuclear fusion applications. *Journal of Nuclear Materials* 2018, 511, 544–5552. https://doi.org/10.1016/j.jnucmat.2018.06.017
13. Protik, N.H.; Katre, A.; Lindsay, L.; et al. Phonon thermal transport in 2H, 4H and 6H silicon carbide from first principles. *Materials Today Physics* 2017, 1, 31–38. https://doi.org/10.1016/j.mtphys.2017.05.004
14. Lu, X.G.; Selleby, M.; Bo, S. Calculations of thermophysical properties of cubic carbides and nitrides using the Debye-Grüneisen model. *Acta Materialia* 2007, 55, 1215–1226. https://doi.org/10.1016/j.actamat.2006.05.054
15. Kittel, C. Introduction to Solid State Physics, 7th ed. Wiley; 1997.
16. Kresse, G.; Hafner. J. Ab initio molecular dynamics for liquid metals. *Physical Review B* 1993, 47, 558–561. https://doi.org/10.1103/PhysRevB.47.558

17. Kresse, G.; Furthmüller, J. Efficiency of ab-initio total energy calculations for metals and semiconductors using a plane-wave basis set. *Computational Materials Science* 1996, 6, 15–50. https://doi.org/10.1016/0927-0256(96)00008-0
18. Kresse, G.; Furthmüller, J. Efficient iterative schemes for ab initio total-energy calculations using a plane-wave basis set. *Physical Review B* 1996, 54, 11169–11186. https://doi.org/10.1103/PhysRevB.54.11169
19. Perdew, J.P.; Burke, K.; Ernzerhof, M. Generalized gradient approximation made simple. *Physical Review Letters* 1996, 77, 3865–3868. https://doi.org/10.1103/PhysRevLett.77.3865
20. Monkhorst, H.J.; Pack, J.D. Special points for Brillouin-zone integrations. *Physical Review B* 1976, 13, 5188–5192. https://doi.org/10.1103/PhysRevB.13.5188
21. Kresse, G.; Joubert, D. From ultrasoft pseudopotentials to the projector augmented-wave method. *Physical Review B* 1999, 59, 1758–1775. https://doi.org/10.1103/PhysRevB.59.1758
22. Lindsay, L.; Hua, C.; Ruan, X.L.; et al. Survey of ab initio phonon thermal transport. *Materials Today Physics* 2018, 7, 106–120. https://doi.org/10.1016/j.mtphys.2018.11.008
23. Li, W.; Carrete, J.; Katcho, N.A.; et al. ShengBTE: A solver of the Boltzmann transport equation for phonons. *Computer Physics Communications* 2014, 185, 1747–1758. https://doi.org/10.1016/j.cpc.2014.02.015
24. Li, W.; Lindsay, L.; Broido, D.A.; et al. Thermal conductivity of bulk and nanowire $Mg_2Si_xSn_{1-x}$ alloys from first principles. *Physical Review B* 2012, 86, 174307. https://doi.org/10.1103/physrevb.86.174307
25. Islam, M. A comprehensive investigation on the physical properties of SiC polymorphs for high-temperature applications: A DFT study based on GGA and hybrid HSE06 exchange correlation functionals. *Nuclear Materials and Energy* 2024, 38, 101631. https://doi.org/10.1016/j.nme.2024.101631
26. Nowak, S. Crystal lattice dynamics of various silicon-carbide polytypes. In: Proceedings of the International Conference on Solid State Crystals 2000; October 9–13, 2000; Zakopane, Poland. pp. 181–186.
27. Stockmeier, M.; Müller, R. Sakwe, S.A.; et al. On the lattice parameters of silicon carbide. *Journal of Applied Physics* 2009, 105, 033519. https://doi.org/10.1063/1.3074301
28. Langpoklakpam, C.; Liu, A.C.; Chu, K.H.; et al. Review of silicon carbide processing for power MOSFET. *Crystals* 2022, 12, 245. https://doi.org/10.3390/cryst12020245
29. Islam, M.; Sarker, M.S.I.; Nakamura, T.; et al. Structural, electronic and magnetic properties of $L1_0$ ordered CoPt nanoparticles: An experimental and DFT study. *Materials Chemistry and Physics* 2021, 269, 124727. https://doi.org/10.1016/j.matchemphys.2021.124727
30. Snead, L.L.; Nozawa, T.; Katoh, Y.; et al. Handbook of SiC properties for fuel performance modeling. *Journal of Nuclear Materials* 2007, 371, 329–377. https://doi.org/10.1016/j.jnucmat.2007.05.016
31. Feldman, D.W.; Parker, J.H.; Choyke, W.J.; et al. Phonon dispersion curves by Raman scattering in SiC, polytypes 3C, 4H, 6H, 15R, and 21R. *Physical Review* 1968, 173, 787–793. https://doi.org/10.1103/PhysRev.173.787
32. Parlinski, K.; Li, Z.Q.; Kawazoe, Y. First-principles determination of the soft mode in cubic ZrO_2. *Physical Review Letters* 1997, 78 4063–4066. https://doi.org/10.1103/PhysRevLett.78.4063
33. Hua, Y.; Bai, W.; Dai, S.; et al. Maldistribution of chemical bond strength inducing exceptional anisotropy of thermal conductivity in non-layered materials. *Angewandte Chemie International Edition* 2023, 62, e202303081. https://doi.org/10.1002/anie.202303081
34. Stacey, F.D.; Hodgkinson, J.H. Thermodynamics with the Grüneisen parameter: Fundamentals and applications to high pressure physics and geophysics. *Physics of the Earth and Planetary Interiors* 2019, 286, 42–68. https://doi.org/10.1016/j.pepi.2018.10.006
35. Boehler, R.; Ramakrishnan, J. Experimental results on the pressure dependence of the Grüneisen parameter: A review. *Journal of Geophysical Research: Solid Earth* 1980, 85, 6996–7002. https://doi.org/10.1029/JB085iB12p06996
36. Qian, X.; Jiang, P.Q.; Yang, R.G. Anisotropic thermal conductivity of 4H and 6H silicon carbide measured using time-domain thermoreflectance. *Materials Today Physics* 2017, 3, 70–75. https://doi.org/10.1016/j.mtphys.2017.12.005
37. Tersoff, J. Chemical order in amorphous silicon carbide. *Physical Review B* 1994, 49, 16349–16352. https://doi.org/10.1103/PhysRevB.49.16349
38. Lucas, G.; Bertolus, M.; Pizzagalli, L. An environment-dependent interatomic potential for silicon carbide: calculation of bulk properties, high-pressure phases, point and extended defects, and amorphous structures. *Journal of Physics: Condensed Matter* 2009, 22, 035802. https://doi.org/10.1088/0953-8984/22/3/035802

39. Hitova, L.; Yakimova, R.; Trifonova, E.P.; et al. Heat capacity of 4H-SiC determined by differential scanning calorimetry. *Journal of The Electrochemical Society* 2000, 147, 3546–3548. https://doi.org/10.1016/j.apsusc.2006.10.052
40. Sun, L.; Gao, Y.M.; Yoshida, K.; et al. Prediction on structural, mechanical and thermal properties of Al_4SiC_4, Al_4C_3 and 4H-SiC under high pressure by first-principles calculation. *Modern Physics Letters B* 2017, 31, 1750080. https://doi.org/10.1142/S0217984917500804